LETTER

doi:10.1038/nature17158

A neuronal circuit for colour vision based on rod–cone opponency

Maximilian Joesch[1] & Markus Meister[2]

In bright light, cone-photoreceptors are active and colour vision derives from a comparison of signals in cones with different visual pigments. This comparison begins in the retina, where certain retinal ganglion cells have 'colour-opponent' visual responses—excited by light of one colour and suppressed by another colour[1]. In dim light, rod-photoreceptors are active, but colour vision is impossible because they all use the same visual pigment. Instead, the rod signals are thought to splice into retinal circuits at various points, in synergy with the cone signals[2]. Here we report a new circuit for colour vision that challenges these expectations. A genetically identified type of mouse retinal ganglion cell called JAMB (J-RGC)[3], was found to have colour-opponent responses, OFF to ultraviolet (UV) light and ON to green light. Although the mouse retina contains a green-sensitive cone, the ON response instead originates in rods. Rods and cones both contribute to the response over several decades of light intensity. Remarkably, the rod signal in this circuit is antagonistic to that from cones. For rodents, this UV-green channel may play a role in social communication, as suggested by spectral measurements from the environment. In the human retina, all of the components for this circuit exist as well, and its function can explain certain experiences of colour in dim lights, such as a 'blue shift' in twilight. The discovery of this genetically defined pathway will enable new targeted studies of colour processing in the brain.

Like most mammals, the mouse has one type of rod and two types of cone photoreceptors, with absorption maxima in the ultraviolet (S pigment) and green (M pigment) region of the spectrum. As in other small mammals, the retinal organization of the cones is inhomogeneous: the M and S pigments are largely segregated in the dorsal and ventral retina, respectively[4]. At the level of ganglion cells, the spectral sensitivity essentially follows this cone distribution[5,6], which severely limits any local comparison of signals across cone pigments. Because behavioural experiments show that mice can indeed 'see colour'[7], it has been suggested that colour vision in mice operates on very different principles from primates[8]. Surprisingly, as we demonstrate here, the mouse does have a dedicated ganglion cell type with clearly opponent responses to light of different wavelengths. It uses an unexpected retinal circuit that circumvents the obstacle caused by the spatial segregation of cone pigments.

We recorded the visual responses of J-RGCs in the retina of a mouse line that labels these neurons fluorescently[3] (Fig. 1a). When probed with white light, the receptive field has OFF-type sensitivity in the centre and ON-type sensitivity in the surround (Fig. 1b). As reported previously, the surround is stronger on the side of the asymmetric dendritic arbor[3]. Stimulation using coloured lights led to a surprise. Many J-RGCs produce an OFF response to uniform UV light, but an ON response to green light (Fig. 1c). The UV-OFF response arises in the receptive field centre and is driven almost entirely by the S pigment (S-OFF), whereas the Green-ON response derives from the surround from almost pure M pigment (M-ON) (Fig. 1d–f and Extended Data Fig. 1a).

A survey of J-RGCs across the retina revealed diversity in their spectral sensitivities (Fig. 2a, b and Extended Data Fig. 1). The receptive field centre reflects the dorsoventral cone opsin gradient[5] (Fig. 2c), S-OFF ventrally and M-OFF dorsally. The surround, however, had an M-ON spectrum regardless of retinal location (Fig. 2a, b). Focusing

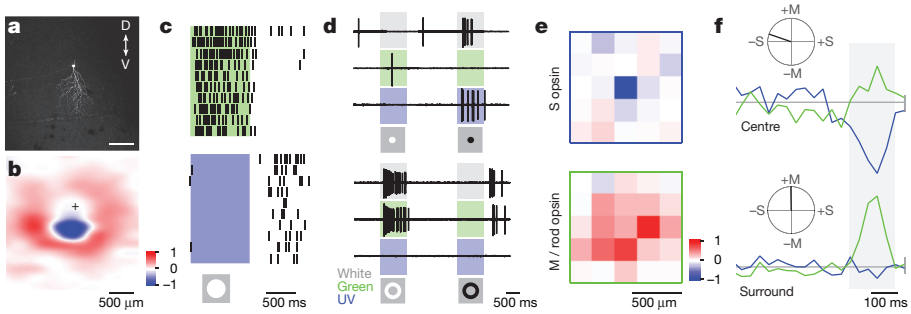

Figure 1 | A spectrally opponent pathway in the mouse retina. **a**, A fluorescent J-RGC in a whole-mounted retina from a JAM-B-CreER; Thy1-STOP-YFP double transgenic mouse. D, dorsal, V, ventral. **b**, Spatial receptive field of a different J-RGC obtained by reverse correlation of the intracellular voltage to an achromatic random flicker stimulus (see Methods). Cross indicates soma position. Polarity: red, ON; blue, OFF. **c**, Raster graph of a spectrally opponent J-RGC response to either full field green (top) or UV (bottom) light stimuli (with green adapting background light). **d**, Response to a flashed spot (top, 250 µm diameter) or annulus (bottom 2,000 µm and 350 µm for outer and inner diameter, respectively) centred on the receptive field using UV, green, or white (UV + green) light. **e**, Spatial receptive field (see Methods) split into contributions from S opsin (top) and M/rod opsin (bottom). Polarity: red, ON; blue, OFF. **f**, Temporal filter (normalized) for the receptive field centre (top, centre pixel in **e**) and surround (bottom, average of the 8 pixels surrounding the centre in **e**) for S opsin and M/rod opsin (blue and green traces, respectively). Graph reports the average opsin activation that occurred as a function of time before a spike. Inset: opsin-space polar graph of the chromatic sensitivity in centre (top) and surround (bottom) calculated from the mean values of the M and S curves in the shaded interval (−198 to −33 ms). For example '+M' indicates a pure M-ON response.

[1]Harvard University, 52 Oxford Street, Cambridge, Massachusetts 02138, USA. [2]Division of Biology and Biological Engineering, California Institute of Technology, Pasadena, California 91125, USA.

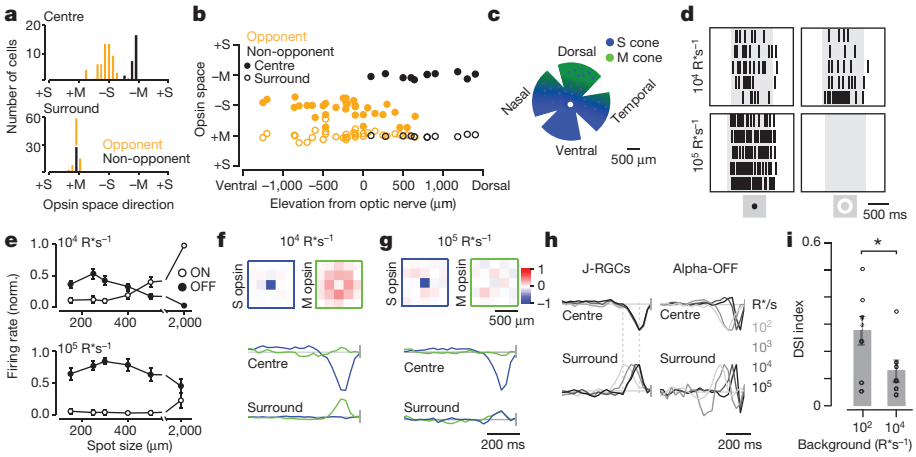

Figure 2 | Rod–cone antagonism. a, Histogram of chromatic sensitivity for centre (top) and surround (bottom) responses of all J-RGCs ($n = 96$). The angle in opsin space is derived as in Fig. 1f. Black, non-opponent cells; orange, opponent cells. **b**, Opsin contributions to the receptive field centre and surround plotted as a function of dorsoventral position. **c**, Cone opsin distribution in a schematic retina drawn with four incisions[5]; (blue, S opsin; green, M opsin; dots, pure S cones). **d**, Response to flashes at intermediate (10^4 R*s^{-1}) and high (10^5 R*s^{-1}) intensity. Achromatic OFF-spots (left, 250 μm diameter) drive the RF centre, and ON-annuli (right, 2,000 μm and 350 μm for outer and inner diameter, respectively) drive the surround. Raster graph of spikes on 5 trials. **e**, Center-surround antagonism for spectrally opponent J-RGCs, at intermediate (top) and high (bottom) intensity. Each curve shows the peak firing rate in response to flashed spots of increasing size, measured separately at light onset (ON) and offset (OFF). Data were normalized for each cell and averaged over 7–12 cells (mean ± s.e.m.). **f**, **g**, Time-course and spatial profile of the receptive field at photopic intensities of 10^4 R*s^{-1} (**f** is normalized to a common peak value and averaged over 67 cells) and 10^5 R*s^{-1} (**g**, 20 cells), displayed as in Fig. 1e, f. **h**, Time-course for centre and surround responses acquired at four mean intensities (10^2, 10^3, 10^4 and 10^5 R*s^{-1}, grey to black), and normalized to a common peak value. Left, J-RGCs (averaged over 8–20 cells); surround kinetics speed up by 125 ms with increasing light intensity (dotted lines), whereas centre kinetics do not. Right, OFF-sustained alpha cells (5 cells). **i**, Direction selectivity of J-RGCs at low and high background intensity. The direction selectivity index (Methods) to small spots moving in eight directions is plotted for each J-RGC, along with mean ± s.e.m. *$P < 0.05$, one-way ANOVA.

attention on the spectrally opponent J-RGCs in the ventral retina, their M-sensitive surround poses a puzzle because the ventral retina is thought to be largely devoid of M-type cones[4]. The only green-sensitive pigment available there in abundance is the rhodopsin in rods. Its absorption spectrum is close to that of the M-cone pigment and indistinguishable by our spectral analysis (Figs 1 and 2 and Extended Data Fig. 2).

To test whether the surround is driven by rods, we systematically varied the absolute light level of the visual stimuli. At light levels that cause isomerization of ~1 rhodopsin per rod per second (1 R*s^{-1}) the sensitivity of rods begins to decline following Weber's law until they cease to function at ~10^5 R*s^{-1} (refs 9 and 10). At intensities of ~10^2 R*s^{-1}, cones are effectively more sensitive than rods, and gradually take over visual signalling[9,11]. As predicted, an annulus flashed on the surround at mean intensities of 10^4 R*s^{-1} still produced ON responses, but at tenfold higher intensity this response was lost (Fig. 2d). By contrast, the centre OFF response strengthened at the highest intensity (Fig. 2d). A weak antagonistic surround remained at the highest light levels, suppressing the OFF response by about 40% from its peak (Fig. 2e). This suppression had a contribution from the S opsin (Fig. 2g), which was not detectable at lower intensities (Fig. 2f). Thus it appears that the antagonistic surround of J-RGCs is mostly driven by rods. Non-opponent J-RGCs in the dorsal retina, however, seem to be less dominated by rods (Extended Data Fig. 3a–c).

At low intensities, the surround response was strong, but considerably slower than that of the centre (Fig. 2h, 10^2 R*s^{-1}). Increasing the light level accelerated the kinetics to approach the centre response (Fig. 2h, 10^5 R*s^{-1}), which retained the same kinetics throughout this intensity range. Because the rod response is considerably slower than that of cones[12], this observation suggests that the surround draws on a rod-driven pathway that gradually saturates at the highest light levels, whereas the centre response is dominated by cones throughout. For comparison we recorded from ON- and OFF-sustained alpha-RGCs, because they can be identified easily by their large soma size and sustained centre response[5,13]. In these RGC types, the kinetics of both centre and surround accelerated with increasing light level, indicating that both receptive field regions receive substantial rod signals (Fig. 2h).

For the J-RGC, the weakening of the surround at high light levels has a strong impact on another functional characteristic—its direction selectivity. This direction preference arises largely from an interaction between the receptive field centre and the asymmetric surround[3]. Consistent with this, we found that adaptation to a background that weakens the surround abolished much of the direction preference to moving spots (Fig. 2i).

To explore the retinal circuits underlying spatial and chromatic opponency in ventral J-RGCs, we voltage-clamped the cells and measured their synaptic currents driven by chromatic stimuli in different parts of the receptive field. The results revealed an even more intricate form of opponency. Both excitatory and inhibitory currents individually have spectrally opponent centre-surround receptive fields. The excitation has a polarity of S-OFF in the centre and M-ON in the surround, whereas inhibition is S-ON in the centre and M-OFF in the surround (Fig. 3a, b and Extended Data Figs 4a and 5). The excitatory current from the receptive field centre most likely reflects glutamate release from type 1 or 2 OFF-bipolar cells[14], whose terminals co-stratify with the dendrites of the J-RGC at the outer margin of the inner plexiform layer[3]. The antagonistic surround of the excitatory current could derive either via direct excitation from ON-bipolar cells that synapse *en passant* onto the J-RGC dendrites or via suppression of the excitatory input from OFF-bipolar cells. The excitatory surround survived pharmacological block of the ON-pathway (Fig. 3d, top right, and 3f) and even simultaneous block of the two inhibitory transmitters GABA and glycine, pointing to the latter hypothesis (Fig. 3e, right, and Extended Data Figs 4c and 5m–o). The only lateral inhibition circuit known to function under such extreme conditions is feedback via horizontal cells to the cones that drive the centre bipolar cells[15] (Fig. 3g).

The inhibitory current driven by the receptive field centre is dependent on GABAergic transmission (Fig. 3c, bottom left, and Extended Data Figs 4b and 5g–l) and thus derives from an ON-amacrine cell type. Block of transmission at the synapse to ON-bipolars eliminated

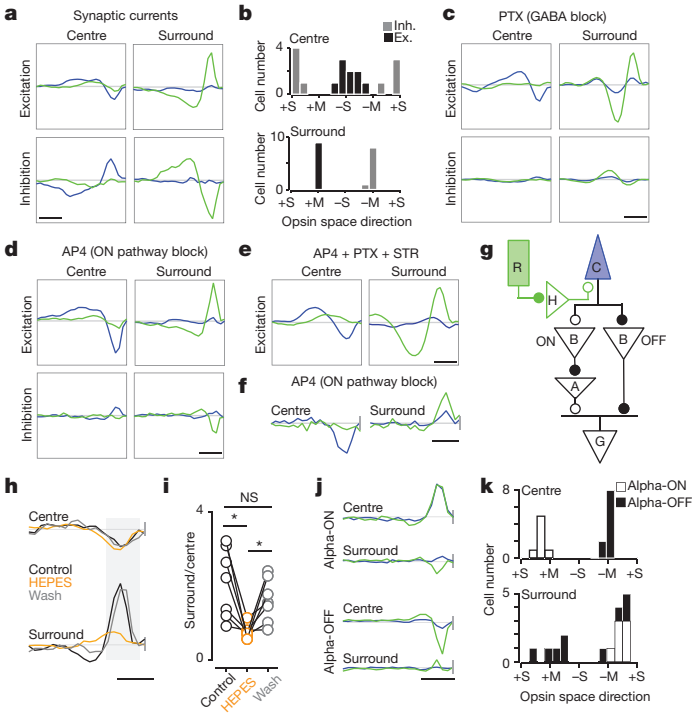

Figure 3 | Synaptic pathways for spectral opponency. a, Visual sensitivity of synaptic currents recorded from J-RGCs under voltage clamp. Excitatory (top) and inhibitory (bottom) conductances are driven by stimulation of the centre (left) or surround (right) of the receptive field. Each curve represents the sensitivity of the conductance to stimulation of the M/rod pigment (green) or S pigment (blue) at various times in the past (normalized to the combined excitation and inhibition, see Methods). Data are from ventral J-RGCs (average of $n = 9$ spectrally opponent cells), where rod and cone signals can be discerned by their spectral sensitivity, but the analysis of dorsal non-opponent J-RGCs yielded similar conclusions (Extended Data Fig. 3d, e). **b**, Histogram of the chromatic sensitivity for centre (top) and surround (bottom) currents (black, excitation; grey, inhibition) recorded from many J-RGCs, displayed by the angle in opsin space, as in Fig. 2a. **c**, As in **a**, but during block of GABA receptors with picrotoxin (PTX; 100 μM; $n = 7$). Although the loss of GABAergic inhibition alters the kinetics of excitatory signals, the centre-surround antagonism remains. **d**, As in **a**, but during block of ON-bipolar responses with L-AP4 (11 μM; $n = 11$). **e**, As in **a**, but during combined block of GABA and glycine receptors and ON-bipolar pathways (100 μM PTX, 10 μM strychnine, 11 μM L-AP4; $n = 7$). **f**, Spiking responses, displayed as in Fig. 1f ($n = 8$) during L-AP4 application. **g**, Working model of neural circuits underlying the response of J-RGCs (G), involving rods (R), cones (C), horizontal cells (H), bipolar cells (B), and amacrine cells (A). Open/closed circles denote inhibitory/excitatory synapses. **h**, Visual sensitivity of spiking responses (average of $n = 7$) in control solution (black), 20 mM HEPES (orange), and after wash-out (grey). **i**, Change in the centre-surround ratio from HEPES exposure calculated from the mean values in the shaded interval in **h** (−198 to −33 ms). **j**, Visual sensitivity of spiking responses from sustained alpha ON−RGCs (average of $n = 7$) and sustained alpha OFF−RGCs (average of $n = 11$). Sensitivity plotted as in Fig. 2f for stimulation of S opsin (blue) and M/rod opsin (green). **k**, Histogram of the chromatic sensitivity for centre (top) and surround (bottom) recorded from alpha ON−RGCs and alpha OFF−RGCs. Display as in Fig. 2a. Scale bars, 200 ms.

~80% of the inhibition (Fig. 3d, bottom left, and Extended Data Fig. 5a–f), indicating that the receptive field centre drives inhibition through ON-bipolars via GABAergic ON-amacrines (Fig. 3g). Again, these inhibitory currents showed an antagonistic OFF-surround, and those responses had the same pharmacological sensitivity as the centre signals (Fig. 3c, bottom right and 3d, bottom right), requiring both the ON-pathway and GABAergic transmission. This suggests that centre and surround use the same bipolar cell pathways and the antagonistic surround already arises in the outer retina as suggested above. We propose that the receptive field centre is implemented by a cone-selective push-pull system of OFF-bipolars and narrow-field ON-amacrines. The surround derives from lateral inhibition of the cones via horizontal cells with rod input (Fig. 3g).

The horizontal cell of the mouse retina connects to cones at the dendritic tree near the soma and to rods at the terminal arborization of its axon. It has been claimed that the thin axon and a high somatic membrane conductance preclude any flow of signals between the soma and terminal compartments[16]. However, transmission from soma to terminal[17] and in the opposite direction has been observed directly[18]. To specifically test the role of horizontal cells we blocked their feedback by applying the pH buffer HEPES[19]. This strongly reduced the surround, on average fourfold relative to the centre response (Fig. 3h, i). At rod-saturating light levels, the horizontal cell should still implement lateral inhibition among cones, and indeed the surround has a UV-sensitive component under those conditions (Fig. 2g). One could imagine additional surround circuits in the inner retina that make use of the ON-type rod bipolar cell, but we found that J-RGCs remain spectrally opponent even under block of all ON-bipolar responses (Fig. 3f).

If the rod-driven surround does arise already at the cone terminal, then one would expect to see the effects in other ganglion cell types. Most of the sustained alpha cells we recorded in the ventral retina indeed showed a surround dominated by the rod pigment (Fig. 3j, k). Unique to the J-RGCs is a centre pathway that is perfectly selective for cones, even under conditions where the rods are clearly active. To test this notion under extreme conditions, we recorded from J-RGCs in a mutant background (*Gnat2*^{cpfl3}) where the cones are silent owing to a transducin mutation. We found that the receptive field centre of J-RGCs had little or no detectable light sensitivity, whereas the surround responded strongly to rod signals (Extended Data Fig. 6). Thus, we conclude that spectral opponency in the mouse retina arises already in certain bipolar cells, by virtue of their cone-selective inputs[20].

The mesopic range of luminance, in which both rods and cones are signalling, spans 0.02–20 cd m^{-2}, namely from dim moonlight to bright twilight[21]. Mice are active under all of these conditions. Although the mouse is commonly considered as strictly nocturnal, in the wild they tend to seek food during the day[22]. A further constraint on this colour

channel is that it can function only in the part of the retina containing S pigment. In a mouse with a head posture typical during locomotion, that part covers the entire superior visual field, dipping below the horizon[23] to include nearby points on the ground.

To explore what ecological benefits mice might draw from colour vision, we searched for objects in the natural world that would stand out in this spectrally opponent channel. Using a modified camera that approximates the absorption of S and M rod pigments, we screened for salient UV-green coloured objects under natural light. Certain seeds and urine marks stand out by being relatively bright or dark in UV[24], respectively (Extended Data Fig. 7). A spot of dry mouse urine is barely detectable from the background with the human eye, but has fourfold higher contrast (Extended Data Fig. 8) when processed by a spectrally opponent system like the J-RGC. Beyond its obvious excretory role, urine serves an important function for social communication among mice. Males mark their territories by squirting urine in characteristic patterns; these marks are sampled and counter-tagged by other individuals, and communicate information regarding social status. Interpretation of the tag requires physical contact because the relevant pheromones are non-volatile[25]. In the wild, mice tag their territory with accumulation of urine and solid matter that lead to sizable vertical structures called urine posts[26]. As expected, this material is dark in the UV (Extended Data Fig. 7d, e). Mice use primarily visual cues to recognize their territory boundaries[27]. On that background, we propose that mice in the wild can identify urine tags visually, using the UV-green opponent colour channel of the retina, which assists in approaching the tag.

In the human retina, the type-1 horizontal cell offers a similar route for opponency between rods and cones. Interestingly, it predominantly contacts the L and M cones over S cones[28]. Therefore, when rods are active in dim light, L and M activity should be suppressed, shifting the spectral balance towards signals from S cones. This may explain the pronounced blue shift we experience in twilight and night-time scenes, and the general observation that 'rod-colour is blue'[29]. Finally, certain individuals lack L and M cones entirely. Nonetheless they report percepts of colour, and psychophysical experiments confirm that they experience a two-dimensional colour space, spanned by the signals from rods and blue cones[30]. We suggest that these 'blue-cone monochromats' use the same rod-cone circuits as the mouse J-RGC for opponent-colour processing.

Online Content Methods, along with any additional Extended Data display items and Source Data, are available in the online version of the paper; references unique to these sections appear only in the online paper.

Received 29 March 2015; accepted 21 January 2016.
Published online 6 April 2016.

1. Solomon, S. G. & Lennie, P. The machinery of colour vision. *Nature Rev. Neurosci.* **8,** 276–286 (2007).
2. Völgyi, B., Deans, M., Paul, D. & Bloomfield, S. Convergence and segregation of the multiple rod pathways in mammalian retina. *J. Neurosci.* **24,** 11182–11192 (2004).
3. Kim, I.-J. J., Zhang, Y., Yamagata, M., Meister, M. & Sanes, J. R. Molecular identification of a retinal cell type that responds to upward motion. *Nature* **452,** 478–482 (2008).
4. Baden, T. *et al.* A tale of two retinal domains: near-optimal sampling of achromatic contrasts in natural scenes through asymmetric photoreceptor distribution. *Neuron* **80,** 1206–1217 (2013).
5. Chang, L., Breuninger, T. & Euler, T. Chromatic coding from cone-type unselective circuits in the mouse retina. *Neuron* **77,** 559–571 (2013).
6. Wang, Y. V., Weick, M. & Demb, J. B. Spectral and temporal sensitivity of cone-mediated responses in mouse retinal ganglion cells. *J. Neurosci.* **31,** 7670–7681 (2011).
7. Jacobs, G. H., Williams, G. A. & Fenwick, J. A. Influence of cone pigment coexpression on spectral sensitivity and color vision in the mouse. *Vision Res.* **44,** 1615–1622 (2004).
8. Jacobs, G. H., Williams, G. A., Cahill, H. & Nathans, J. Emergence of novel color vision in mice engineered to express a human cone photopigment. *Science* **315,** 1723–1725 (2007); comment **318,** 196 (2007).
9. Naarendorp, F. *et al.* Dark light, rod saturation, and the absolute and incremental sensitivity of mouse cone vision. *J. Neurosci.* **30,** 12495–12507 (2010).
10. Soucy, E., Wang, Y., Nirenberg, S., Nathans, J. & Meister, M. A novel signaling pathway from rod photoreceptors to ganglion cells in mammalian retina. *Neuron* **21,** 481–493 (1998).
11. Williams, G. A., Daigle, K. A. & Jacobs, G. H. Rod and cone function in coneless mice. *Vis. Neurosci.* **22,** 807–816 (2005).
12. Nikonov, S. S., Kholodenko, R., Lem, J. & Pugh, E. N. Jr Physiological features of the S- and M-cone photoreceptors of wild-type mice from single-cell recordings. *J. Gen. Physiol.* **127,** 359–374 (2006).
13. Pang, J.-J., Gao, F. & Wu, S. M. Light-evoked excitatory and inhibitory synaptic inputs to ON and OFF alpha ganglion cells in the mouse retina. *J. Neurosci.* **23,** 6063–6073 (2003).
14. Euler, T., Haverkamp, S., Schubert, T. & Baden, T. Retinal bipolar cells: elementary building blocks of vision. *Nature Rev. Neurosci.* **15,** 507–519 (2014).
15. Thoreson, W. B. & Mangel, S. C. Lateral interactions in the outer retina. *Prog. Retin. Eye Res.* **31,** 407–441 (2012).
16. Nelson, R., von Litzow, A., Kolb, H. & Gouras, P. Horizontal cells in cat retina with independent dendritic systems. *Science* **189,** 137–139 (1975).
17. Trümpler, J. *et al.* Rod and cone contributions to horizontal cell light responses in the mouse retina. *J. Neurosci.* **28,** 6818–6825 (2008).
18. Szikra, T. *et al.* Rods in daylight act as relay cells for cone-driven horizontal cell-mediated surround inhibition. *Nature Neurosci.* **17,** 1728–1735 (2014).
19. Hirasawa, H. & Kaneko, A. pH changes in the invaginating synaptic cleft mediate feedback from horizontal cells to cone photoreceptors by modulating Ca^{2+} channels. *J. Gen. Physiol.* **122,** 657–671 (2003).
20. Tsukamoto, Y., Morigiwa, K., Ueda, M. & Sterling, P. Microcircuits for night vision in mouse retina. *J. Neurosci.* **21,** 8616–8623 (2001).
21. Nathan, J. *et al.* Scotopic and photopic visual thresholds and spatial and temporal discrimination evaluated by behavior of mice in a water maze. *Photochem. Photobiol.* **82,** 1489–1494 (2006).
22. Daan, S. *et al.* Lab mice in the field: unorthodox daily activity and effects of a dysfunctional circadian clock allele. *J. Biol. Rhythms* **26,** 118–129 (2011).
23. Sterratt, D. C., Lyngholm, D., Willshaw, D. J. & Thompson, I. D. Standard anatomical and visual space for the mouse retina: computational reconstruction and transformation of flattened retinae with the Retistruct package. *PLoS Comput. Biol.* **9,** e1002921 (2013).
24. Tovée, M. J. Ultra-violet photoreceptors in the animal kingdom: their distribution and function. *Trends Ecol. Evol.* **10,** 455–460 (1995).
25. Hurst, J. L. & Beynon, R. J. Scent wars: the chemobiology of competitive signalling in mice. *Bioessays* **26,** 1288–1298 (2004).
26. Welch, J. F. Formation of urinating posts by house mice (*Mus*) held under restricted conditions. *J. Mamm.* **34,** 502–503 (1953).
27. Mackintosh, J. H. Factors affecting recognition of territory boundaries by mice (*Mus musculus*). *Anim. Behav.* **21,** 464–470 (1973).
28. Ahnelt, P. & Kolb, H. Horizontal cells and cone photoreceptors in human retina: a Golgi-electron microscopic study of spectral connectivity. *J. Comp. Neurol.* **343,** 406–427 (1994).
29. Stabell, U. & Stabell, B. Mechanisms of chromatic rod vision in scotopic illumination. *Vision Res.* **34,** 1019–1027 (1994).
30. Reitner, A. & Sharpe, L. T. Is colour vision possible with only rods and blue-sensitive cones. *Nature* **352,** 798–800 (1991).

Acknowledgements We thank E. Soucy and J. Greenwood for technical support, J. Cauceglia for providing the urine post samples, J. R. Sanes and E. Soucy for comments on the manuscript. This work was supported by grants to M.M. from the NIH and to M.J. from The International Human Frontier Science Program Organization.

Author Contributions M.J. designed the study, performed all experiments, interpreted results, and wrote the manuscript. M.M. helped design the study, interpret results, and wrote the manuscript.

Author Information Reprints and permissions information is available at www.nature.com/reprints. The authors declare no competing financial interests. Readers are welcome to comment on the online version of the paper. Correspondence and requests for materials should be addressed to M.M. (meister@caltech.edu) or M.J. (joeschkrotki@fas.harvard.edu).

METHODS

Data reporting. No statistical methods were used to predetermine sample size. The experiments were not randomized. The investigators were not blinded to allocation during experiments and outcome assessment.

Histology. For the image in Fig. 1a, the retina was drop-fixed with 4% paraformaldehyde in PBS for 2 h on ice, washed with PBS and blocked with 3% goat serum/0.1% Triton X-100/PBS overnight. For staining, tissue was incubated with 3% goat serum/0.1% Triton X-100/PBS and rabbit anti-GFP Alexa Fluor 488 conjugate (dilution 1:1,000, Invitrogen, A-21311) at 4°C for 3 days and washed with PBS. Retina was mounted on Vectashield mounting medium (Vectorlabs) and imaged in a confocal microscope (Olympus FVA).

Animals. Animals were used in accordance with NIH guidelines and protocols approved by Institutional Animal Use and Care Committee at Harvard University. Mice were maintained on a C57/B6J background. Both male and female mice were used in this study. Animals were 40 to 150 days old at the time of euthanasia. To visualize J-RGCs, JAMB-Cre-ER mice were mated to Thy1-STOP-YFP transgenic mice[3]. To activate Cre and thereby YFP, 3 mg of tamoxifen (dissolved in sunflower oil at 50 mM; W530285 & T5648; Sigma) was injected at least twice intraperitoneally at between P10 and P21. Gnat2^{cpfl3} mice[31] were obtained from Jackson Laboratories and crossed to JAMB-Cre-ER and Thy1-STOP-YFP.

Recording. The dark-adapted mouse retina was isolated under far-red light (LED peak 735 nm, additionally filtered with a 735 nm LP filter eliciting an isomerization rate of ~17 R*/s) in oxygenated Ames' medium (Sigma) with constant bubbling (95% O_2, 5% CO_2) at room temperature. Four incisions were made to flat-mount the retina with ganglion cells facing up in a superfusion chamber on the stage of a custom-built upright fluorescence microscope. Ganglion cell bodies were visualized using oblique angled IR light (850 nm LED, eliciting isomerization rates <0.01 R*s^{-1}). Spike recordings were obtained with loose cell-attached patch microelectrodes filled with Ames' medium. Current and voltage recordings were made in whole-cell voltage- and current-clamp modes, respectively (Axon Multiclamp 700B). Electrodes had an impedance of 5–8 MΩ and were filled with high potassium internal solution (120 mM KAc, 1 mM NaCl, 0.2 mM $CaCl_2$, 1 mM $MgCl_2$, 10 mM EGTA, 2 mM MgATP, 0.3 mM GTP, 1 mM KCl, 10 mM HEPES) containing an additional 5 mM lidocaine *N*-ethyl bromide (QX314-Br). In pharmacological experiments, agents were bath-applied at the following concentrations: 100 μM picrotoxin, 10 μM strychnine, and 11 μM L-AP4. All chemicals were obtained from Sigma-Aldrich, with exception of QX-314 (EMD Millipore Biosciences). During voltage-clamp recordings, excitatory and inhibitory synaptic currents were separated by voltage clamping the cell to the equilibrium potential of chloride (−65 mV) and unselective cation channels (0 mV), respectively. A junction potential of 12 mV was subtracted. It is possible that conductances in distal dendrites of the J-RGC are incompletely clamped under this protocol, leading to some uncertainty about the assignment of inhibitory and excitatory inputs. However, such errors are likely small, because PTX blocked almost all the inhibitory currents and not the excitatory currents (Fig. 3c). Only cells with an input resistance of 8–25 MΩ were used. The superfusion liquid was heated to 32 °C (Warner TC-324B). Signals were digitized at 10 kHz (National Instruments PCIe-6321), highpass-filtered at 0.1 or 1 Hz, and acquired using software written in LabVIEW (National Instruments). Data were analysed using MATLAB (MathWorks). Fluorescent J-RGCs were detected by brief excitation (64 ms) with a green LED eliciting ~10^6 R*/flash. This flash was followed by up to 20 min of recovery and adaptation to the intended mean luminance level before recordings were initiated. This restored the RGC response properties to the pre-flash condition (Extended Data Fig. 9). After the physiological recordings, the cell's arbor was revealed with longer fluorescence exposures. To determine a neuron's dorsoventral location on the retina, we measured the distance from the soma to the optic nerve and used the dendritic orientation to identify the ventral direction.

Stimulation. Light stimuli were delivered from a modified Dell M109S DLP projector through a custom-made lens system and focused onto the photoreceptors (frame rate 60 Hz, magnification 5.5 μm per pixel, maximal Michelson contrast: 0.995). The projector's blue LED was replaced with a high-power UV-LED (ProLight 1W UV LED, peak 405 nm), to improve the differential stimulation of S and M pigments. Owing to peculiarities of the projector, the green light includes a small component from the UV LED and vice versa (Extended Data Fig. 2). The relative intensities of the green and UV lights were chosen such that the average output of the stimulator matches the spectrum of daylight (Extended Data Fig. 2); this ensures that the retina is in a realistic state of chromatic adaptation. Intensities and spectra were measured using a calibrated spectrometer (Thorlabs CCS-100) and a digital power meter (Thorlabs S130C sensor). Most experiments were performed at a mean photopic intensity of 10^4 R*s^{-1} per rod. When stated otherwise, the light intensity was changed uniformly by exchanging reflective neutral density filters (Thorlabs) in the light path. The respective cone pigment isomerization rates for all light levels used in this study are depicted in Extended Data Fig. 2. Isomerization rates were determined using opsin templates[32] and assuming that the mouse rod has an optical density at peak absorption wavelength of 0.015 μm^{-1}, a length of 24 μm, a diameter of 1.4 μm and a quantum efficiency of 0.67 (refs 33, 34).

A spatiotemporal white-noise stimulus was presented using a binary pseudorandom sequence, in which the two primary lights (green and UV) varied independently. For checkerboard stimuli (Figs 1e, f and 2f, g and Extended Data Figs. 3b, c and 5), the checker size was 220×220 μm^2. For the achromatic white-noise stimulus, checker dimensions were 60×60 μm^2, and the green and UV lights were flickered synchronously (Fig. 1b). For the spot-annulus flicker stimuli, the centre spot had a diameter of 250 μm, and the surround annulus had inner and outer diameters of 350 μm and 2,000 μm, respectively; spot and annulus were separated by a constant grey annulus (Fig. 3 and Extended Data Figs 3d, e and 4). All white-noise stimuli were presented at 30 Hz update rate. Spot-annulus flashes were presented with the same stimulus dimensions. For coloured flash experiments, either the UV or the green light were changed from an average white background (both lights at half intensity, Fig. 1d and Extended Data Figs 1 and 4a). In achromatic stimuli, both lights were changed together (Fig. 2d and Extended Data Fig 4b, c). Full-field chromatic stimuli were presented on a green adapting background to reduce M opsin excitation from UV light via the β-band; UV spot and annulus flashes were presented without background (Fig. 1c). Moving spot stimuli consisted of a white spot (width 250 μm, 2×10^4 R*s^{-1}) on a grey background (either 50 R*s^{-1} or 10^4 R*s^{-1}) moved through the receptive field centre in eight different directions chosen randomly and repeated 3 times per experiment with a 1 s pause between sweeps at 800 μm s^{-1} (Fig. 2i).

Analysis. The response to flashing spots or annuli was quantified by counting spikes in the interval between 0.1 s and 1 s after the onset or the offset of the flash, and normalizing to the maximum value obtained. The resulting relative response strength was then averaged across cells (Fig. 2e and Extended Data Fig. 3a). In voltage clamp experiments (Extended Data Fig. 4), the difference between the peak of the stimulus-evoked current and the mean value in the 500 ms interval prior the stimulus onset was analysed.

To measure the response to moving spots, we averaged the spike count over several trials with identical sweeps of the spot. From experiments with eight directions (separated by 45°), the direction selectivity index (DSI) was calculated from the response-weighted vector sum of all directions:

$$\mathrm{DSI} = \frac{|\sum_k r(\varphi_k) e^{i\varphi_k}|}{\sum_k r(\varphi_k)} \quad (1)$$

Where φ_k is the angle of the kth direction and $r(\varphi_k)$ is the corresponding spike rate. This index ranges from 0 for a cell with equal responses to all directions to 1 for a cell that responds to only one direction (Fig. 2i).

The spatiotemporal receptive fields were computed starting with reverse-correlation functions to the randomly flickering stimulus:

$$h(\mathbf{x}, t) = \frac{1}{T}\int_0^T r(t')s(\mathbf{x}, t'+t)dt' \quad (2)$$

where T represents the duration of the recording; $s(\mathbf{x}, t)$ represents the stimulus at location $\mathbf{x}$ and time t; and $r(t)$ represents the response at time t.

The response variable $r(t)$ is either the firing rate, namely the number of spikes per stimulus update interval (Figs 1e, f, 2f–h and 3f, h–j and Extended Data Figs 3b, c and 9), or the membrane potential (Fig. 1b), or membrane currents (Fig. 3a, c–e and Extended Data Figs 3d and 5). The stimulus variables are the normalized intensity of the green or UV lights:

$$s_l = \frac{I_l - \bar{I}_l}{\bar{I}_l}, l = G(\text{green}) \text{ or } U(\text{UV}) \quad (3)$$

where

I_l = intensity of light l
$\bar{I}_l$ = average intensity of light l

From these two correlation functions we derived the sensitivity of the response to modulation of the S and M pigments. Note that the mouse has 3 photoreceptor types, but the rod and M cone have very similar absorption spectra (peak wavelength $\lambda_{max} = 502$ nm versus 508 nm) that cannot be resolved by our methods. For simplicity, we refer to this common spectral sensitivity as 'M opsin', bearing in mind that any response components with that spectral sensitivity may derive from the M cone or from the rod. We arrive at that distinction by independent methods, as described in the text.

Each of the two lights of the stimulator drives both pigments, though in different ratios. To make the conversion, we model the response as

$$r = r_0 + c_S \frac{I_S - \bar{I}_S}{\bar{I}_S} + c_M \frac{I_M - \bar{I}_M}{\bar{I}_M} \quad (4)$$

where

r_0 = baseline response

$\frac{I_p - \bar{I}_p}{\bar{I}_p}$ = Weber contrast for photoreceptor type p, $p = M$ or S

c_p = sensitivity to photoreceptor type p

By evaluating the reverse-correlation to the two lights, h_U and h_G, predicted from this linear model one finds the relation

$$\begin{aligned} h_U &= c_S E_{SU} + c_M E_{MU} \\ h_G &= c_S E_{SG} + c_M E_{MG} \end{aligned} \quad (5)$$

where

$$E_{pl} = \frac{e_{pl}}{e_{pU} + e_{pG}}$$

e_{pl} = isomerization rate in photoreceptor p under average light l

Finally, the respective photoreceptor contributions to the response are

$$\begin{pmatrix} c_S \\ c_M \end{pmatrix} = \mathbf{E}^{-1} \cdot \begin{pmatrix} h_U \\ h_G \end{pmatrix}, \text{ where } \mathbf{E} = \begin{pmatrix} E_{SU} & E_{MU} \\ E_{SG} & E_{MG} \end{pmatrix} \quad (6)$$

In general, these opsin contributions to the response were computed for every location and time point, yielding $c_S(\mathbf{x}, t)$ and $c_M(\mathbf{x},t)$ (as in Fig. 1e). For a specific location and time (for example, Fig. 1f) we represented the ratio of the two opsin contributions by the 'opsin space angle'

$$\varphi = \arg(c_S + i \cdot c_M) \quad (7)$$

Camera and spectra. We assembled the UV/Green imaging device using a monochromatic camera (Point Grey, FL3-U3-13Y3M-C) with a CMOS chip sensitive over the band 350–950 nm (min 30% of peak sensitivity). We used fused silica lenses (Thorlabs) that are transparent over 200–1,200 nm. Light was filtered using two different band-pass filters that overlap to ~70% with the mouse M and S bands (BP390 #86-348 and BP510 #84-097, Edmund Optics). Images were taken separately in the two bands and adjusted to compensate for the camera's sensitivity to different wavelengths and for chromatic aberration. The illumination was indirect sunlight (Extended Data Fig. 7). Spectra were acquired using a calibrated spectrometer (Thorlabs CCS-100). The spectra in Extended Data Fig. 7f were calculated using opsin templates[32] and multiplied by the transmission spectrum of the mouse eye[35].

31. Chang, B. *et al.* Cone photoreceptor function loss-3, a novel mouse model of achromatopsia due to a mutation in *Gnat2*. *Invest. Ophthalmol. Vis. Sci.* **47,** 5017–5021 (2006).
32. Govardovskii, V. I., Fyhrquist, N., Reuter, T., Kuzmin, D. G. & Donner, K. In search of the visual pigment template. *Vis. Neurosci.* **17,** 509–528 (2000).
33. Carter-Dawson, L. D. & LaVail, M. M. Rods and cones in the mouse retina. I. Structural analysis using light and electron microscopy. *J. Comp. Neurol.* **188,** 245–262 (1979).
34. Penn, J. S. & Williams, T. P. A new microspectrophotometric method for measuring absorbance of rat photoreceptors. *Vision Res.* **24,** 1673–1676 (1984).
35. Henriksson, J. T., Bergmanson, J. P. & Walsh, J. E. Ultraviolet radiation transmittance of the mouse eye and its individual media components. *Exp. Eye Res.* **90,** 382–387 (2010).

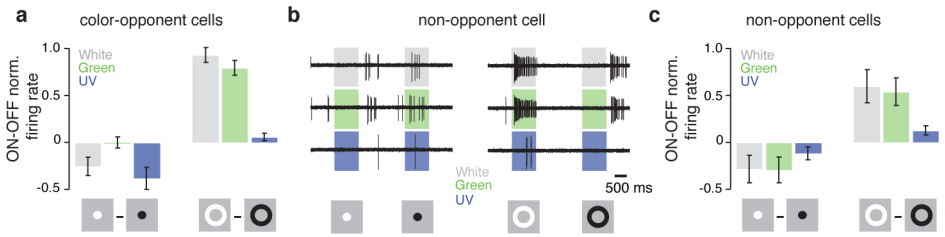

Extended Data Figure 1 | Spiking responses to chromatic centre and surround stimuli. a, Summary of responses to centre (left) and surround (right), derived from the experiment of Fig. 1d. Peak firing rate to an ON flash was subtracted from that to the OFF flash, and averaged over cells ($n = 7$; mean ± s.e.m.). Green light acts almost exclusively in the surround, UV light only in the centre. **b**, Response of a non-opponent J-RGC to a flashed spot or annulus (as in Fig. 1c). **c**, Summary of the differential response for non-opponent cells ($n = 8$, ± s.e.m.) displayed as in **a**. Green light and UV light act with the same polarity, OFF in centre, ON in surround. Note that both lights excite the M cone that is prevalent in the dorsal retina.

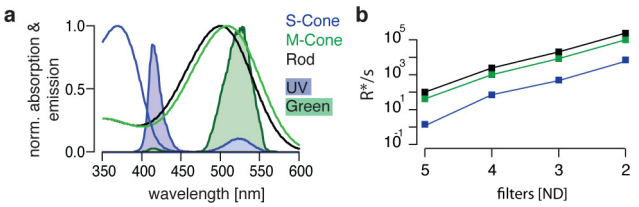

Extended Data Figure 2 | Spectra of the visual stimuli. a, Normalized absorption spectra of mouse photoreceptors (black trace: rhodopsin; green: M opsin; blue: S opsin). Overlaid, the normalized emission spectra of the UV and green light emitted by the DLP projector (filled blue: UV, filled green: green light). **b**, Isomerization rate per photoreceptor in rods (black), M cones (green) and S cones (blue). The collecting area for cones was 0.2 μm^2, for rods see Methods.

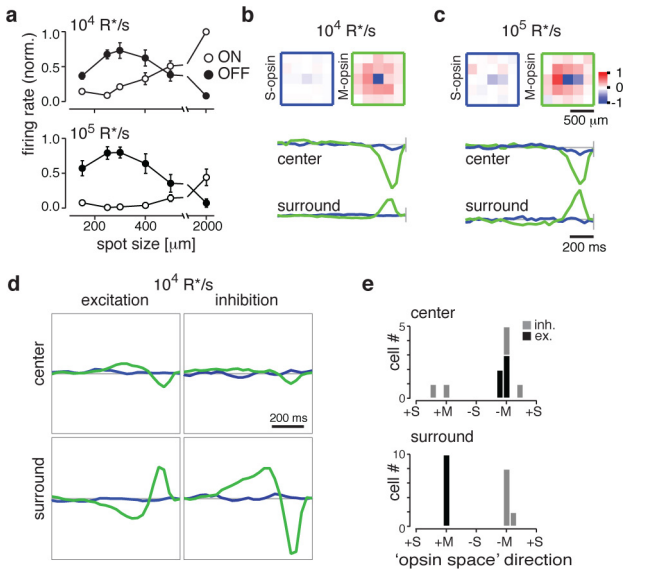

Extended Data Figure 3 | Responses of non-opponent J-RGCs in dorsal retina. a, Centre surround antagonism for non-opponent J-RGCs, at intermediate (top) and high (bottom) intensity. Each curve shows the peak firing rate in response to flashing spots of increasing size, measured separately at light onset (ON) and offset (OFF). Data were normalized for each cell and averaged over 7–14 cells (mean ± s.e.m.). **b**, **c**, Time course and spatial profile of the receptive field at different photopic intensities, averaged over 20 or 32 cells, respectively, and displayed as in Fig. 1e, f. **d**, Time course of excitatory (left) and inhibitory (right) conductance changes from stimulation of the S (blue trace) and M/rod-pigments (green) in the receptive field centre (top) and surround (bottom) (non-opponent cells $n = 5$, displayed as in Fig. 3a). **e**, Opsin space histogram for centre (top) and surround (bottom) currents (black: excitation, grey: inhibition). Note similarity to results from opponent J-RGCs (Fig. 3), except that the centre is driven by M pigment, as expected given the paucity of S cones in the dorsal region. The surround again has a pure M spectrum and produces both presynaptic and post-synaptic inhibition, with dynamics that are virtually identical to the signals in ventral J-RGCs.

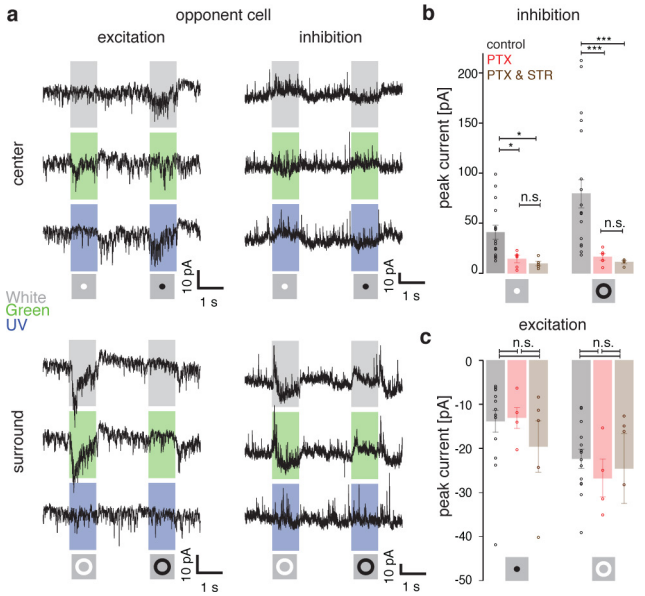

Extended Data Figure 4 | J-RGC current responses to flashed spots and annuli. a, Inhibitory and excitatory currents of a spectrally opponent J-RGC to a flashed spot (top, 250 μm diameter) and annulus (bottom, 2,000 μm and 350 μm for outer and inner diameter, respectively) centred on the receptive field using UV, green, or white (green + UV) light. **b**, **c**, Peak currents measured to a white flashed spot and annulus (**b**, inhibition, ON spot & OFF annulus; **c**, excitation, OFF spot & ON annulus; stimulus dimensions as in a) in control (black), picrotoxin (PTX, 100 μM; red), and combined (brown) PTX (100 μM) and strychnine (STR, 10 μM). Circles: individual cells; means ± s.e.m.; n.s.: not significant, $*P < 0.05$, $***P < 0.001$, one-way ANOVA. Note the synaptic currents in J-RGCs are systematically smaller (for example, excitatory current from centre stimulation = 10–20 pA) than those measured in other RGC types (for example, 500–1,000 pA typical in sustained alpha cells) during the same recording session.

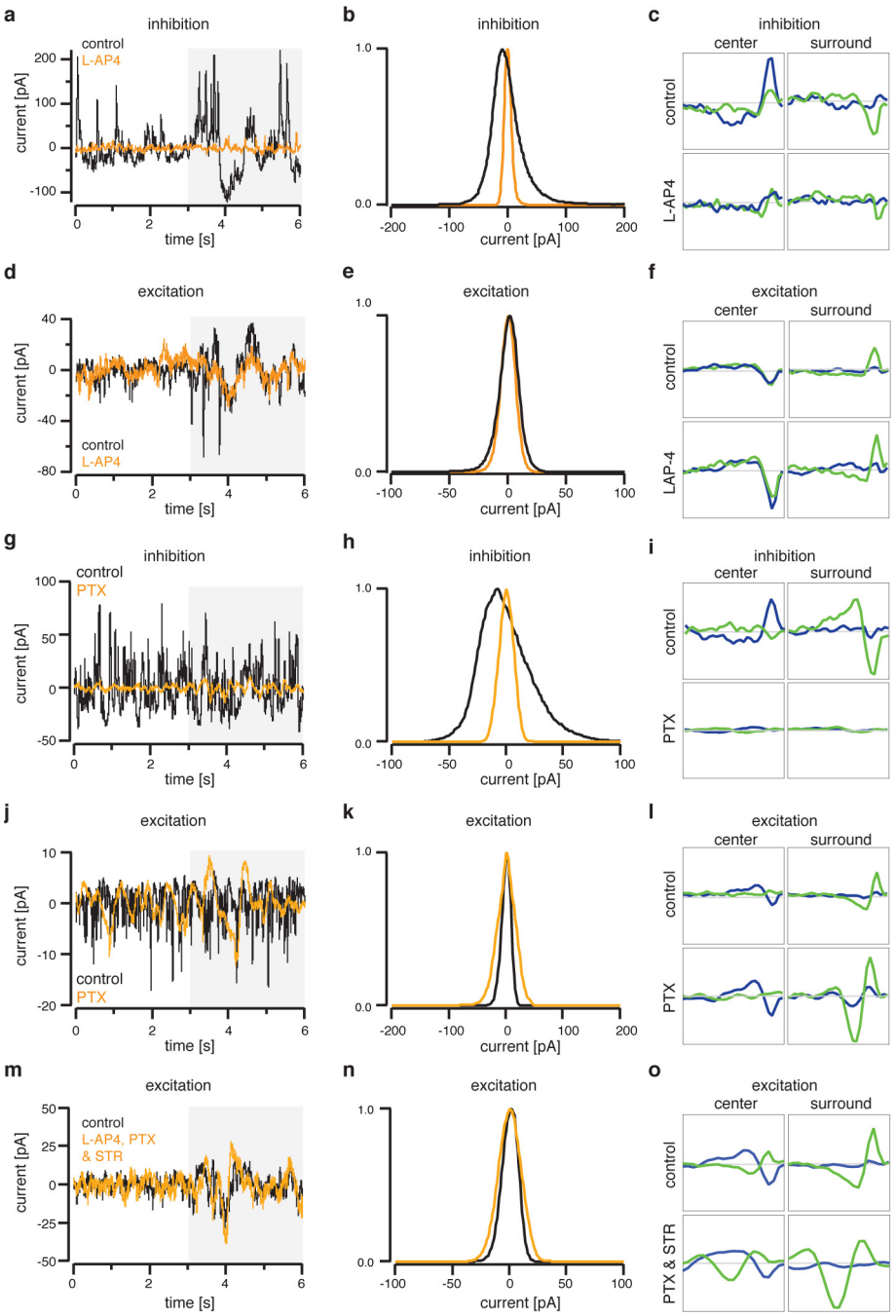

Extended Data Figure 5 | Synaptic pathways for spectral opponency (single cell examples). a, **d**, **g**, **j**, **m**, Inhibitory and excitatory currents during white-noise flicker stimulation of three different J-RGCs before and after drug application (shaded grey depicts the start of white-noise stimulus; **a**, **d**, L-AP4 11 μM; **g**, **j**, PTX 100 μM; **m**, L-AP4 11 μM, PTX 100 μM and STR 10 μM). **b**, **e**, **h**, **k**, **n**, Single cell excitatory and inhibitory current distribution under white-noise stimulation (before and during drug application). Inhibitory current distribution is dramatically narrowed during L-AP4 and PTX application, the excitatory current distribution remains comparatively unaltered. **c**, **f**, **i**, **l**, **o**, Single cell visual sensitivity of synaptic currents recorded from the respective J-RGC recordings in the left panels (as in Fig. 3a). Excitatory and inhibitory conductances are driven by stimulation of the centre (left) or surround (right) of the receptive field. Each curve represents the sensitivity of the conductance to stimulation of the M/rod pigment (green) or S pigment (blue) at various times in the past (see Methods).

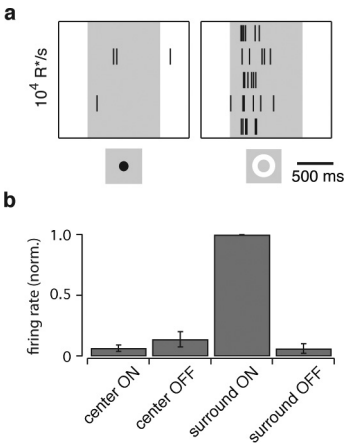

Extended Data Figure 6 | J-RGCs in a mutant retina with silenced cones. Responses of J-RGCs in the ventral retina of homozygous *Gnat2*^{cpfl3} mutant mice. Flashing spots and annuli as in Fig. 1d. **a**, Raster graph of spiking for one sample neuron. **b**, Summary of responses from 5 neurons. Firing rate normalized to that under 'surround ON' stimulation. Note little or no response to centre stimulation. Compare to wild-type retina in Figs 1d and 2d and Extended Data Fig. 1.

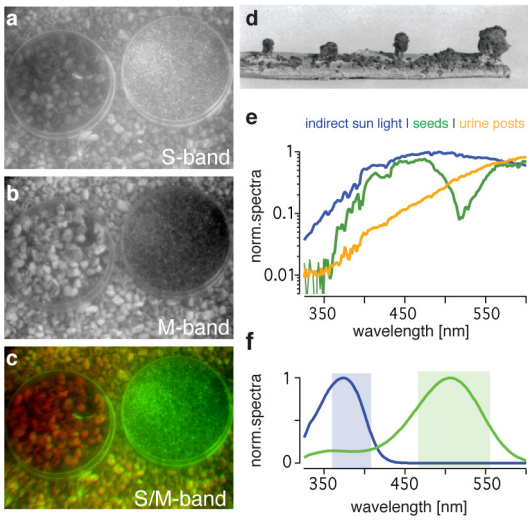

Extended Data Figure 7 | Spectrally opponent features in the environment. Dried mouse urine and plant seeds have high S-M chromatic contrast. **a**–**c**, On a background of clean mouse bedding are two dishes containing bedding soiled with urine (left) and a mix of plant seeds (right). Photographs used a band-pass filter in the ultraviolet (**a**) and in the green (**b**); **c** merges the two using red-green encoding. **d**, Close-up view of mouse urinating posts (reproduced with permission from ref. 26; 2.5–3.5 cm high). **e**, Normalized spectra of indirect sunlight and light reflected from a mixture of untreated plant seeds and urine posts. **f**, Pigment absorption curves for S opsin (blue) and M opsin (green) multiplied by the ocular transmission spectrum (see Methods). Shaded region indicates pass band of the filters used for **a**–**c**.

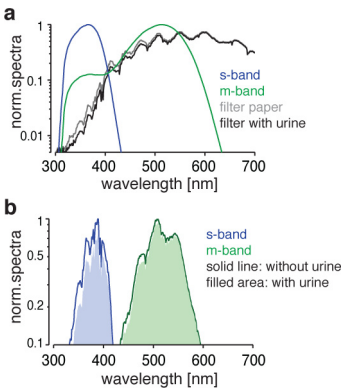

Extended Data Figure 8 | UV-green colour signature of urine. a, Pigment absorption curves for S opsin (blue) and M opsin (green) multiplied by the ocular transmission spectrum (see Methods) and spectra of light reflected from a Whatman filter paper, with or without dried urine marks, under indirect sunlight. **b**, Normalized curves of the product between the above absorption and reflectance spectra. Blue: S opsin, green: M opsin, solid line: clean filter paper, filled area: filter paper with urine. Note that the reduction in the S-band is 27.4%, compared to only 8.2% for the M-band.

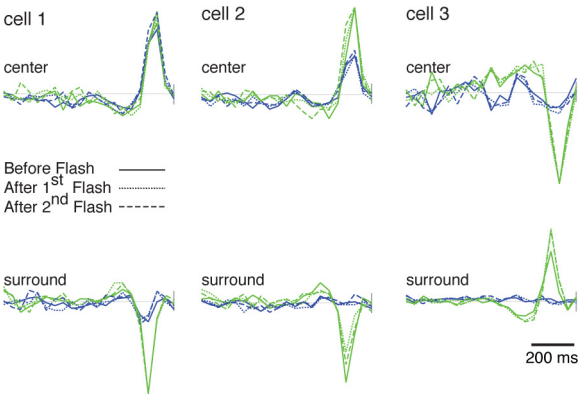

Extended Data Figure 9 | Effects of the light flash exposure for fluorescent targeting. Temporal filter in the receptive field centre and surround for S opsin and M/rod opsin (as in Fig. 1f; blue and green traces, respectively) of three RGCs taken before and after one or two brief light flashes. These neurons were targeted blindly and are therefore not of the J-RGC type. They rely on both rods and cones (note different spectral sensitivity in the centre and surround). Yet their response properties were not altered by the brief flashes.